European Review for Medical and Pharmacological Sciences 2023; 27: 7416-7430

Impact of glycogen synthase kinase-3ß inhibition on rats' temporomandibular joint collagen-induced rheumatoid arthritis with correlation to *miRNA-155/miRNA-24* expression

R.H. AL-SERWI[1], G. OTHMAN[2,3], A.F. DAWOOD[4], A.K. ALHUMAIDAN[1], H.S. ALHARBI[1], M. EL-SHERBINY[2], M.E. ALMADANI[5], D.M.A. ELSHERBINI[6,7]

[1]Department of Basic Dental Sciences, College of Dentistry, Princess Nourah bint Abdulrahman University, Riyadh, Saudi Arabia
[2]Department of Basic Medical Sciences, College of Medicine, AlMaarefa University, Riyadh, Saudi Arabia
[3]Biochemistry Department, Faculty of Medicine, Mansoura University, Mansoura, Egypt
[4]Department of Basic Medical Sciences, College of Medicine, Princess Nourah bint Abdulrahman University, Riyadh, Saudi Arabia
[5]Department of Clinical Medical Sciences, College of Medicine, AlMaarefa University, Riyadh, Saudi Arabia
[6]Department of Clinical Laboratory Sciences, College of Applied Medical Sciences, Jouf University, Sakaka, Saudi Arabia
[7]Department of Anatomy, Faculty of Medicine, Mansoura University, Mansoura, Egypt

Abstract. – OBJECTIVE: The current study considered assessing the role of *miRNA-155* and *miRNA-24* in collagen-induced rheumatoid arthritis (RA) in rats' temporomandibular joint (TMJ). Their role in histological aggressiveness of the disease and therapy response to glycogen synthase kinase (GSK) inhibitor 4-benzyl-2-methyl-1,2,4-thiadiazolidine-3,5-dione (TDZD-8) will be studied.

MATERIALS AND METHODS: Rats were randomly distributed to four groups (8 rats/group): group I negative control, group II collagen-induced rheumatoid arthritis (CIA), group III Control+TDZD-8 treated group, and group IV CIA+TDZD-8 treated group. Then were euthanized 42 days after the start of the experiment. H&E staining, Masson trichrome staining, and immunohistochemical antibodies against S100 were performed. qRT-PCR of *miRNA-155* and *miRNA-24* were done for frozen synovial tissues.

RESULTS: Histological analysis showed that the most affected structure in induced rheumatoid arthritis of TMJ is the articular disc, condylar head, and subchondral bone. Combined treatment with TDZD-8 improved histological status in the joint. Masson's trichrome (MTC) histochemical staining revealed disarrangement of collagen fibers and adherence between the articular disc and condylar cartilage. Meanwhile, the morphology and collagen composition of the disc and condyle in CIA+ TDZD-8 were similar to those of healthy tissues. Immunohistochemical analysis for S100A4 revealed increased immunoreactivity staining in the CIA group. The immunoreactivity was significantly decreased in CIA+ TDZD-8 treated group. TDZD-8 significantly decreased the levels of *miRNA-155* and *miRNA-24* in synovial tissue.

CONCLUSIONS: Our results reveal for the first-time correlation of *miRNA-155* and *miRNA-24* that might be implicated in the onset of TMJ RA. Consequently, the treatment of CIA with GSK inhibitor (TDZD-8) yields encouraging results. We predicted the TDZD-8 might protect against CIA by suppressing *miRNA-155*, miRNA-24, and S100A4 protein levels.

Key Words:
Temporomandibular, Rheumatoid arthritis, GSK-3b inhibitors, TDZD-8, *miRNA-155*, *miRNA-24*.

Introduction

One of human joints' long-lasting, degenerative inflammatory disorders is rheumatoid arthritis (RA)[1]. Its pathogenesis still needs to be fully clarified; evidence states that interaction between environmental, genetic, and immunologic factors contribute to the disease[2]. Both innate and adaptive immunity are implicated, and macrophages and T-cells have an imperative role in its pathogenic mechanism[3]. The temporomandibular joint (TMJ) is a compound synovial joint composed of the temporal bone's glenoid fossa and the mandibular condyle with interposed articular disc[4]. The most prevalent

Corresponding Author: Dalia Mahmoud Abdelmonem Elsherbini, MD; e-mail: dmelsherbini@ju.edu.sa

type of inflammation-related arthritis linked to TMJ malfunction is this one[5]. The overall incidence of rheumatoid arthritis-related TMD is underestimated, owing in most cases to a shortage of a routine rheumatologist assessment for TMD in the rheumatology practice[6]. Sadura-Sieklucka et al[7] reported that 50% of RA patients have TMJ dysfunction according to evaluation by the visual analog pain scale and TMJ palpation. Studies[8] indicate that between 19-85.7% of RA patients have TMJ abnormalities and symptoms in the form of joint discomfort, swelling, restricted jaw mobility, and even ankylosis.

Proteoglycan degeneration and weariness in the fibrocartilage of the articular eminence and condylar head are two key abnormalities that may be identified[9]. Eventually, Cortical and subcortical bone destruction result in condylar damage associated with subchondral bone and osteoclastic bone destruction[10]. In later stages, joint stiffness with limited movement and muscle spasms were prominent[11].

Rheumatoid factor (RF) has been detected as the primary serological test for diagnosing RA[12]. Recently, Anti-citrullinated peptide antibody (ACPA) tests were developed and made commercially available[13]. Since ACPA exist prior to the start of RA manifestations and is indicative of the RA progression, they are a valued diagnostic tool early in the prognosis of the disease[14].

Micro-RNAs (miRNAs) which are small non-coding RNAs (18-23 nucleotides in length) have been found to control the pre- and post-translational levels of gene expression in a variety of targets[15]. It has been evident over the past few years that RA patients exhibit changes to their cellular (miRNAs)[16]. In RA synovial tissue and synovium macrophages, *miRNA-155* was shown to be highly expressed[17]. Its overexpression elicited the production of chemokines and cytokines intensely involved in RA synovitis, namely interleukin-1β (IL-1β), interleukin-6 (IL-6), interleukin-8 (IL-8), and tumor necrosis factor-α (TNF-α)[18]. *miRNA-24* was established to be interrelated to RA pathogenesis through the Human Regulatory T Cells (Treg) pathway, and it is raised in arthritic disorders, including RA. Researchers[19] have revealed that *miRNA-24* is increased in all RA synovial fibroblast samples and synovial fluid as well.

Glycogen synthase kinase 3-β (GSK-3β) is a serine/threonine kinase characterized by site-specific dependent phosphorylation. In the literature[20] was demonstrated that GSK-3 is tangled in various biological functions, including tumorigenesis, cell cycle progression, apoptosis and viability, cytoskeletal organization, and cell metabolism. The inflammation detected in RA is intensely linked with different pro-inflammatory triggers and transcription agents, which had been linked with GSK-3β[21]. The thiadiazolidinone compound TDZD-8 was recognized as a non-adenosine triphosphate (non-ATP) competitive inhibitor of GSK-3β[22]. TDZD-8 has been proven to be a protective mediator in a variety of murine models of disease as arthritis, colitis, spinal cord injury, and septic shock[20]. TDZD-8 can lessen the production of CIA in rats. Also, it can diminish paw edema and bone destruction in RA rats, as presented by the histological analysis of the knee joint[23].

The association between miRNAs and GSK inhibitors has been proven in several pathological processes; GSK-3β is essential in controlling neurogenesis and neuronal survival in the brain[24]. Furthermore, exposure to GSK-3β inhibitors changes the expression of selective miRNAs (upregulated: *miR-144*; downregulated: *let-7b*, *let-7c*, *miR-128a*, *miR-24a*, *miR-30c*, *miR-34a*, and *miR-221*) that target proteins used in neurite outgrowth and neurogenesis[25].

S100 proteins are calcium-binding proteins with a low molecular weight generated by invertebrates[26]. The family comprises more than 20 identified members, detected in various tissues and cells with a pivotal role in several cellular functions[27]. In RA, S100A4, S100A8, s100A9, S100A11, S100A12, and S100B have been associated with inflammatory responses[28]. These S100 proteins might encourage the promotion of arthritis by enhancement of catabolic signaling *via* the receptor for advanced glycation end products (RAGE) in cartilage[29]. S100A4 levels in RA patients are related to radiographic damage and its progression. These proteins might be part of a novel group of biomarkers that predict radiographic progression and poor therapy response in RA patients[30].

Numerous challenges are met during the trip of RA diagnosis and therapy; thus, the current study aims at determining the impact of glycogen synthase kinase-3β inhibition on rats' temporomandibular joint collagen-induced rheumatoid arthritis and correlation to *miRNA-155*/*miRNA-24* Expression. In addition to evaluating the role of *miRNA-155* and *miRNA-24* in TMJ arthritis in rats and the interplay between *miRNA-155*, *miRNA-24*, and S100 protein in the pathogenesis of RA. The present study's findings might help to understand the unexplored role of miRNA in RA pathogenesis, which might add to the diagnostic tests for TMJ arthritis and identify TDZD-8 as a prospective therapeutic drug for managing TMJ arthritis.

Materials and Methods

Animals

Adult male rats, Wistar albino species (170 ± 10 g, 8 weeks of age), were supplied from the animal facility at King Saud University in Riyadh, Saudi Arabia. Rats were accommodated as 4 rats per cage under pathogen-free conditions with ventilation, controlled humidity (50-60%), temperature (22-23°C), and a 12 h light/dark cycle with free access to standard pelleted chow and water. All attempts, including handling, housing, treatment, and operative procedures, were made to ensure proper care of all animals and diminish animal suffering.

Animal Model of Collagen-Induced Arthritis (CIA)

The procedures established by Brand et al[31] were followed to induce the CIA to the assigned groups of rats. Complete Freund's adjuvant (CFA) (Cat. No. F5881, Sigma Aldrich, St. Louis, MO, USA) and Bovine Type II Collagen (CII) (Cat. No. C7806, Sigma Aldrich, St. Louis, MO, USA) were utilized. Collagen II was thawed in diluted acetic acid (10 mM) to a 4 mg/ml concentration by stirring overnight at 4°C. At 4°C, Freund's complete adjuvant was mixed with collagen type II (1:1) to prepare the emulsion. For CIA induction, each rat received an intradermal (i.d.) injection of 100 µL of emulsified collagen type II on day 0 in the skin of the tail, about 1.5 cm distal to the base of the tail. After 14 days, the booster dose was administrated, applying the same concentration and route post-primary immunization. Following this procedure, RA is established in most rats 5-7 days post the second immunization.

Experimental Design

A total of thirty-two adult male rats were arbitrarily distributed into 4 groups (8 rats/group): Group I (control group): rats administrated vehicle of 100 µl normal saline (i.d) on day 0and 14 and then given 100 µl of 0.1% DMSO (i.p) daily from day 21 to day 42; Group II (CIA-induced group): rats with pre-established CIA and received 100 µl of 0.1% DMSO as vehicle from day 21 to day 42; Group III (Control+TDZD-8 treated group): rats were treated as in group I, then treated daily with an i.p dose of 100 µl of 4-benzyl-2-methyl-1,2,4-thiadiazolidine-3,5-dione (TDZD-8), non-ATP competitive inhibitors of glycogen synthase kinase 3β (GSK-3β), (1 mg/kg) (Cat. No. Ab142372, Abcam, Cambridge, UK) starting from day 21 to day 42. Furthermore, Group IV (CIA+TDZD-8-combined treated group): rats with pre-established CIA received an i.p daily dose of 100 µl of TDZD-8 (1 mg/kg) from day 21 to day 42. TDZD-8 was dissolved in diluted DMSO (0.1%). TDZD-8 dose was approved from the previous studies[23]. DMSO of 0.1% has no impact on any of the tested parameters from our preliminary data (data not shown).

Arthritis Scoring

Following the second immunization of CII/CFA, each rat was tested for the prevalence and severity of RA by inspecting the scope of edema and erythema within the four paws starting from day 21 after the first intradermal injection every 2-days.

Inspections were done by two independent researchers who were uninformed of the experiment following the scoring system recognized by Cuzzocrea et al[32]. The average score for the severity of arthritis in each of the hind paws of CIA rats was assessed by two veterinary investigators. The scoring scale was graded from 0-4 with a maximum score of 16.

Biochemical Serum Measurements

By the end of the experiment, all rats were anesthetized with pentobarbital sodium (50 mg/kg, i.p.), the rats' chest was open, and the blood sample was taken *via* cardiac puncture, and then collected in plain tubes, centrifuged at 3,000 rpm to collect serum. Then, rats were killed by cervical dislocation. Rheumatoid Factor (RF) serum levels were determined by a rat's ELISA Kit (Cat. No. CSB-E13666r, CUSABIO Technology LLC, TX, USA). Anti-citrullinated protein antibodies (ACPA) levels in serum were quantified using a rat's ELISA Kit (Cat. No. EKC38678, Biomatik, Ontario, Canada). All measurements followed the manufacturer's instruction.

Synovium Isolation

The heads were fixed in a side position, and the skin was cut apart longitudinally in front of the ear tragus to expose the left TMJ of each rat. Under a dissecting microscope, the soft tissue was removed. To completely expose the synovial tissue, the fibrous/synovial layers were removed. The synovium was harvested, snap-frozen in liquid nitrogen, and stored at -80°C for further use.

Histological and Histochemical Evaluation

The right TMJ tissue was excised and fixated in 4% paraformaldehyde. For demineralization, the samples were placed in gauze bags and

suspended in 10% neutral buffered formalin. This was followed by 10% ethylene diamine tetra acetic acid (EDTA) for demineralization (pH 7). After demineralization was completed, which was assured by a sharp needle piercing the specimen, indicating easy penetration. Each rat's right and left TMJs were dissected and embedded into paraffin blocks. For histological evaluation, deparaffinized 5-µm slices were rehydrated using a graduated ethanol series (100%, 90%, and 70%) and stained with hematoxylin and eosin (H&E)[33] and Masson's trichrome (MTC) staining[34]. Images of histological sections were assessed using a light microscope equipped with a video camera and digital analysis system.

Immunohistochemical Analyses

Deparaffinized and rehydrated 5-µm sections were washed with polybutylene succinate (PBS) and blocked for 30 min in 0.1% H_2O_2 to quench endogenous peroxidase action. Following PBS washing, the sections were incubated for 60 min at room temperature (RT) in a blocking solution (10% normal goat serum). The sections were then incubated with the primary antibody of S100 calcium-binding protein A4 (Anti-S100A4) (Code IS504, Dako A/S, Glostrup, Denmark) at RT for 1 h. Once washed in Tris Buffered Saline (TBS), sections were incubated with a biotinylated secondary antibody for 10 min at RT and rinsed. Next, sections were washed with PBS, and the enzyme conjugate streptavidin-horseradish peroxidase solution was added to the sections for 10 min. Next, sections were washed with PBS, slides stained with two drops (100 µl) of hematoxylin, and then cleaned with distilled water. The slides were finally dehydrated in an ascending graded ethanol series, cleared in xylene, mounted using Histomount, and covered with a coverslip.

Computer-Assisted Morphometric Analysis of Digital Images

Slides were photographed utilizing a digital camera Toupcam (XCAM1080PHA; Toup Tek, Hangzhou, China) fixed on a CX22 Olympus microscope (Olympus, Tokyo, Japan), using 100 and 400 objectives. The output images were assessed *via* Morphology Video Test software (Video Test, St. Petersburg, Russia) with a specified built-in routine for calibrating distance dimension and stain quantification. Five fields from each slide were randomly evaluated (2 slides/rat). Measurements of articular disc thickness were calibrated counter to a micrometer slide. This optical system measures the distance in micrometers (µm) instead of pixels. The measurements were averaged for each image. Images were captured from the camera using a MuTech frame grabber; next, the images' color tones were enhanced depending on the target area's hue. Images were thresholded at the level of the desired hue range to form a binary mask [region of interest (ROI)] that represents target areas. An independent, experienced investigator blindly assessed this. Calculation of percentage area (%A) was applied to obtain the % area of ROI in relation to the total field area. The results were exported in an Excel sheet. The values recorded for 8 animals per group were compared and statistically analyzed.

Quantitative Real-time PCR (qRT-PCR)

Forward primers used to amplify *miR-155* (Cat. No. MPR00417) and *miR-24* (Cat. No. MP-r00003) and Reverse primers (Cat. No. MPH00000) were purchased from ABM (Richmond, Canada). Primers sequence of internal control 18S (Accession No. M11188), F:5-CGGCTACCACATCCAAGGAA-3, R: R: 5GCTGGAATTACCGCGGCT-3) were purchased from Qiagen (Germantown, MD, USA). Total RNA was isoèlated from frozen synovium using an RNeasy Mini Kit (Cat. No. 74104, Qiagen, Victoria, Australia). RNA Purity and concentration were evaluated by calculating the absorbance at 260 and 280 using a NanoDrop ND-1000 spectrophotometer. cDNA was produced by a miRNA All-In-One cDNA Synthesis Kit (Cat. No. G270, ABM, Richmond, Canada). qPCR amplification was done with a CFX96 real-time PCR system (Bio-Rad, Hercules, CA, USA) using BrightGreen miRNA qPCR MasterMix (Cat. No. MasterMix-mS, Quimigen S.L., Madrid, Spain). Reactions of qPCR were made in a total volume of 20 µl/each as follows: 2 µl cDNA and 6 µl Nuclease-free water, 1 µl PCR Forward Primer (final concentration 300 Nm), 1 µl PCR universal Reverse Primer (final concentration 300 Nm),10 µl (1x) Bright Green miRNA qPCR Master Mix, PCR reaction cycles were done for initial 10 min at 95°C, then denaturation 95°C (10 sec), annealing 63°C (15 sec), and extension 72°C (30 sec) for a total of 40 cycles, with a final extension step at 72°C for 5 min. The gene expression levels were calculated by $2^{-\Delta\Delta Cq}$ Livak method. The mRNA expression level was normalized by 18S as an internal control.

Statistical Analysis

Quantitative data were analyzed for normality by performing normality tests (Kolmogorov-Smirnov and Shapiro-Wilk tests). Data were displayed as mean ± (SD) values. A one-way ANOVA test followed by Bonferroni's post-hoc test was applied for parametric data to compare the groups. Kruskal-Wallis test, followed by Dunn's test, was performed for non-parametric data. The significance level was set at $p \leq 0.05$. Statistical analysis was performed with GraphPad Prism version 9 (La Jolla, CA, USA).

Results

Arthritis Index

Figure 1 reveals that the arthritis score of the control and control+TDZD-8 treated groups were zero. The CIA-induced group showed an increase in arthritis scores. The arthritis index of the CIA+TDZD-8 treated group was significantly less than the CIA group throughout the observation period.

H&E Histological Examination

Histological examination of untreated control revealed the typical histological architecture of the TMJ with its articular fossa, articular disc, and condylar head. Histological examination of the untreated control showed typical histological architecture of the TMJ with its articular fossa, articular disc, and condylar head.

The CIA group revealed thickening of the articular disc with fragmentation and splitting between collagen bundles. Thickening of the fibrous layer covering the condyle head with a gradual decline in the condylar cartilage thickness and a number of chondrocytes.

It also revealed destruction and loss of physiological layers of the subchondral bone, widening of bone marrow spaces with evident marrow degeneration, and irregular, disordered trabecular bone. The control+TDZD-8 treated group showed normal anatomical features of the TMJ, similar to those of the untreated group, with no evidence of histological changes. In contrast, CIA+TDZD-8 treated group showed a normal thickness of the articular disc and condylar cartilage and a regular arrangement of bone trabeculae. The thickness of the fibrous layer of the condylar head, temporal bone, and articular disc appeared normal in thickness. The bone marrow spaces of the condylar head showed regeneration with normal histological features (Figure 2A-D).

There was a statistically significant variation between the mean thickness of the articular disc in all groups (p-value = 0.008, Effect size η^2 = 0.556). Pair-wise comparisons using Dunn's test revealed that the CIA group exhibited the statistically significant highest value. There was no statistically significant variation between control, control+TDZD-8, and CIA+TDZD-8 groups; all showed the statistically significantly lowest mean values (Figure 2E).

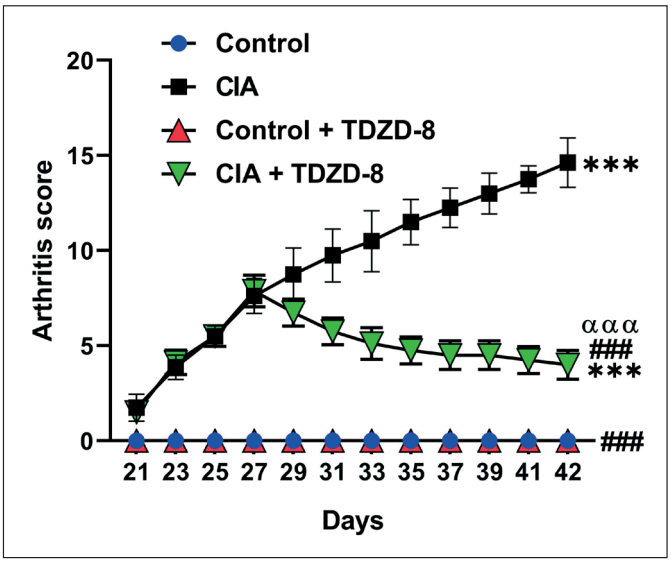

Figure 1. A graph showing arthritis scores in all groups of rats. Data are displayed as the mean (±SD). ***$p <$ 0.001 *vs.* control, $^{###}p < 0.001$ *vs.* CIA, and $^{ααα}p < 0.001$ *vs.* control+TDZD-8.

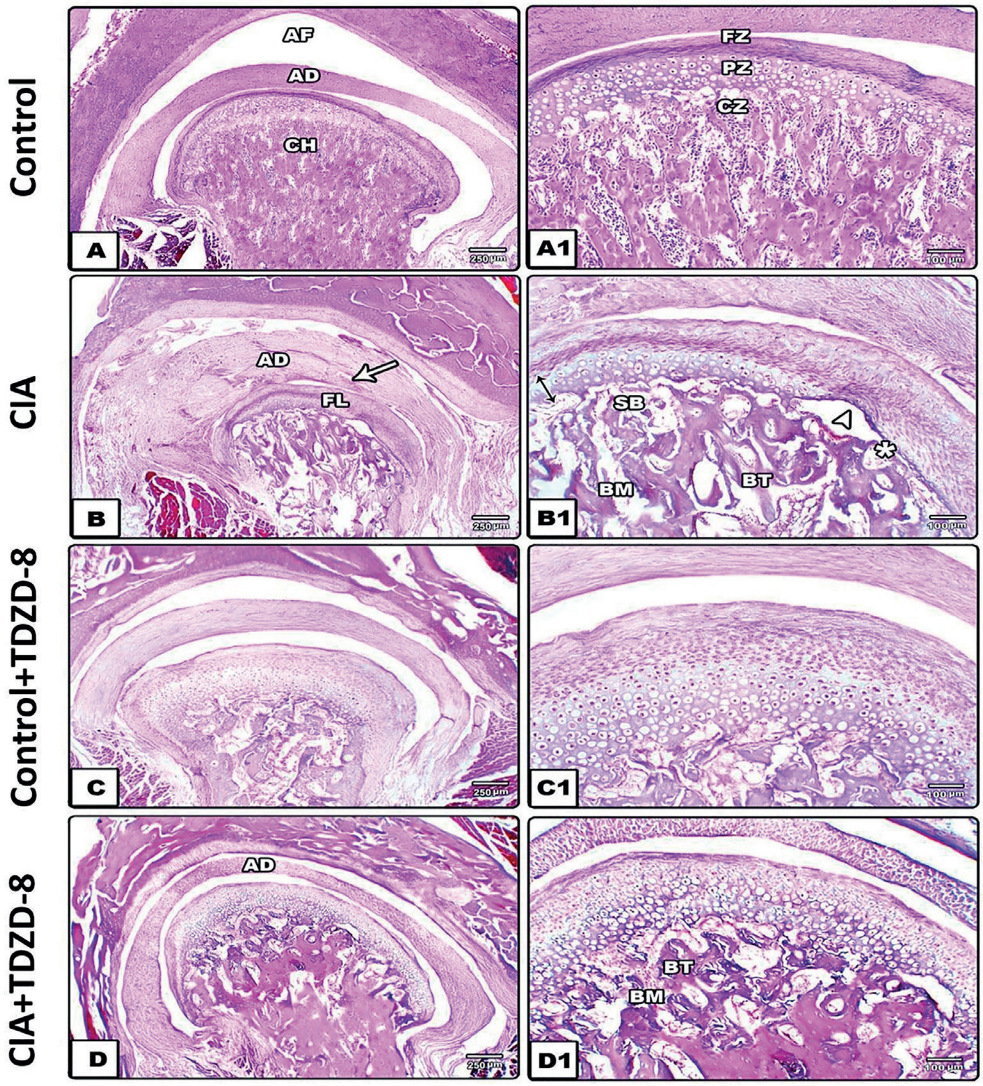

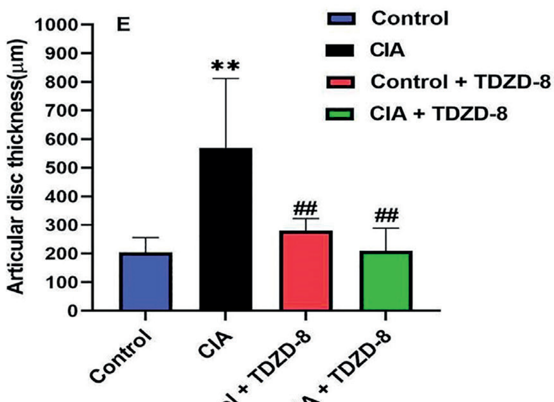

Figure 2. Temporomandibular joint micro-section morphology, H&E staining. **A-A1**, shows normal characteristics of the TMJ, articular fossa (AF), articular disc (AD), and Condylar head (CH) as shown by three distinct zones, an articular zone of fibrous connective tissue (FZ), a proliferative zone containing undifferentiated mesenchymal cells (PZ), a cartilage zone with its chondrocytes (CZ), and the deepest layer including mineralized cartilage and the subchondral bone with its normal regularly architecture. **B-B1**, The CIA-treated group shows thickening of the articular disc (AD) with fragmentation and splitting in between collagen bundles (arrow). The fibrous layer covering the condyle head thickening (FL), the separation between the cartilage and underlying bone (arrowhead) with a gradual decrease in the condylar cartilage thickness (double arrowhead) and chondrocytes number, which is lost in some areas (asterisk). Destruction and Loss of physiological layers of subchondral bone (SB), widening of bone marrow spaces with clear marrow degeneration (BM), and irregular, disordered trabecular bone (BT). **C-C1**, Control+TDZD-8 treated group shows normal anatomical features of the TMJ close similar to (**A-A1**) with no evidence of histological changes. **D-D1**, The CIA +TDZD-8 treated group shows apparently normal articular disc thickness (AD), condylar cartilage, and apparently normal bone trabeculae (BT) arrangement. The thickness of the fibrous layer of the condyle head, temporal bone, and articular disc featured normal. The bone marrow spaces in the condylar head expressed regeneration and normal morphology (BM). Note the separation between the cartilage and underlying bone (arrowhead). The photomicrographs (**A**), (**B**), (**C**), and (**D**) were 100 X magnified, while (**A1**), (**B1**), (**C1**), and (**D1**) were 400 X magnified. **E**, a graph showing the thickness of the articular disc in all groups. Data are shown as the mean (±SD). $^{**}p < 0.01$ *vs.* control, and $^{\#\#}p < 0.01$ *vs.* CIA.

MTC Histochemical Staining Expression

The control group showed normal histological features of collagen fibers distribution, condylar cartilage, and subchondral bone with mineralized regular trabecular bone structures. In the CIA-induced group, a marked increase in positive staining and collagen fibers disarrangement in the articular disc was observed, suggesting the presence of immature collagen fibers. Alterations were more aggravated in the subchondral bone, revealing newly formed unmineralized irregular disordered trabecular bone structures with large marrow cavities close to the cartilage remarkably increased. Changes were more provoked, with side adhesion detected between the articular disc and the condylar cartilage. The control+TDZD-8 treated group showed similar collagen distribution to the untreated group. CIA+TDZD-8 treated group revealed regenerated collagen fibers in some areas of regenerated cartilage; a near-normal arrangement of collagen fibers was observed around cell lacunae (Figure 3A-D).

There was a statistically significant variation between the area percentage of fibrosis in all groups (p-value < 0.001, Effect size $\eta^2 = 0.897$). Pair-wise comparisons using Bonferroni's post-hoc test revealed that the CIA group showed the statistically significantly highest mean area %. Control+TDZD-8 showed statistically significantly lower mean area %. There was no statistically significant difference between the control, CIA+TDZD-8 groups; both showed the statistically significantly lowest mean areas (Figure 3E).

Immunohistochemical Analysis

Immunohistochemical analysis of the CIA group for S100A4 showed an increased expression, characterized by brown discoloration of chondrocytes, predominantly in the deep and, to some extent, in the superficial zone of the non-calcified articular cartilage. Cells in all joints and joint space bone marrow were also strongly positive for S100A4. In contrast, CIA+TDTZ-8 treated group revealed loss of chondrocyte S100A4 immunoreactivity in the non-calcified cartilage and superficial zone compared with group CIA group. However, mild S100 immuno-reactivity was still apparent in the bone marrow of a few osteocytes. Meanwhile, chondrocytes showed little positive S100A4 immunostaining in marginal regions in either control or control+TDZD-8 treated group, although bone marrow and some osteocytes were positive (Figure 4A-D).

There was a statistically significant difference in anti-S100A4 immunohistochemistry area parentage in the four groups (p-value < 0.001, Effect size $\eta^2 = 0.994$). Pair-wise comparisons using Bonferroni's post-hoc test revealed that the CIA group showed the statistically significantly highest mean area %. CIA+TDZD-8 showed statistically significantly lower mean area %. There was no statistically significant difference between control, control+TDZD-8 groups; both showed the statistically significantly lowest mean areas % (Figure 4E).

Rheumatoid Factor (RF) And Anti-Citrullinated Protein Antibodies (ACPA) Serum Levels

There was a statistically significant difference between mean RF levels in the four groups (p-value < 0.001, Effect size $\eta^2 = 0.923$). Pair-wise comparisons using Bonferroni's post-hoc test revealed that the CIA group showed the statistically significantly highest mean RF level. CIA+TDZD-8 group showed a statistically significantly lower mean value. There was no statistically significant difference between the control and control+TDZD-8 groups; both showed the statistically significantly lowest mean RF level (Figure 5A).

There was a statistically significant difference between mean ACPA levels in the four groups (p-value < 0.001, Effect size $\eta^2 = 0.959$). Pair-wise comparisons using Bonferroni's post-hoc test revealed that the CIA group showed the highest mean ACPA level, which was statistically significant. ACPA level declined significantly in the CIA+TDZD-8 group. There was no statistically significant difference between the control and control+ TZD-8 groups; both showed the statistically significantly lowest mean ACPA level (Figure 5B).

Quantitative Real-Time PCR

There was a statistically significant difference between mean *miRNA-155* levels in the four groups (p-value < 0.001, Effect size $\eta^2 = 0.926$). Pair-wise comparisons using Bonferroni's post-hoc test revealed that the CIA group showed the statistically significantly highest mean *miRNA-155* level. There was no statistically significant difference between the control and CIA+TDZD-8 groups; both showed significantly lower mean levels. Control+TDZD-8 group showed the lowest mean *miRNA-155* level with non-statistically significant difference from CIA+TDZD-8 group (Figure 6A).

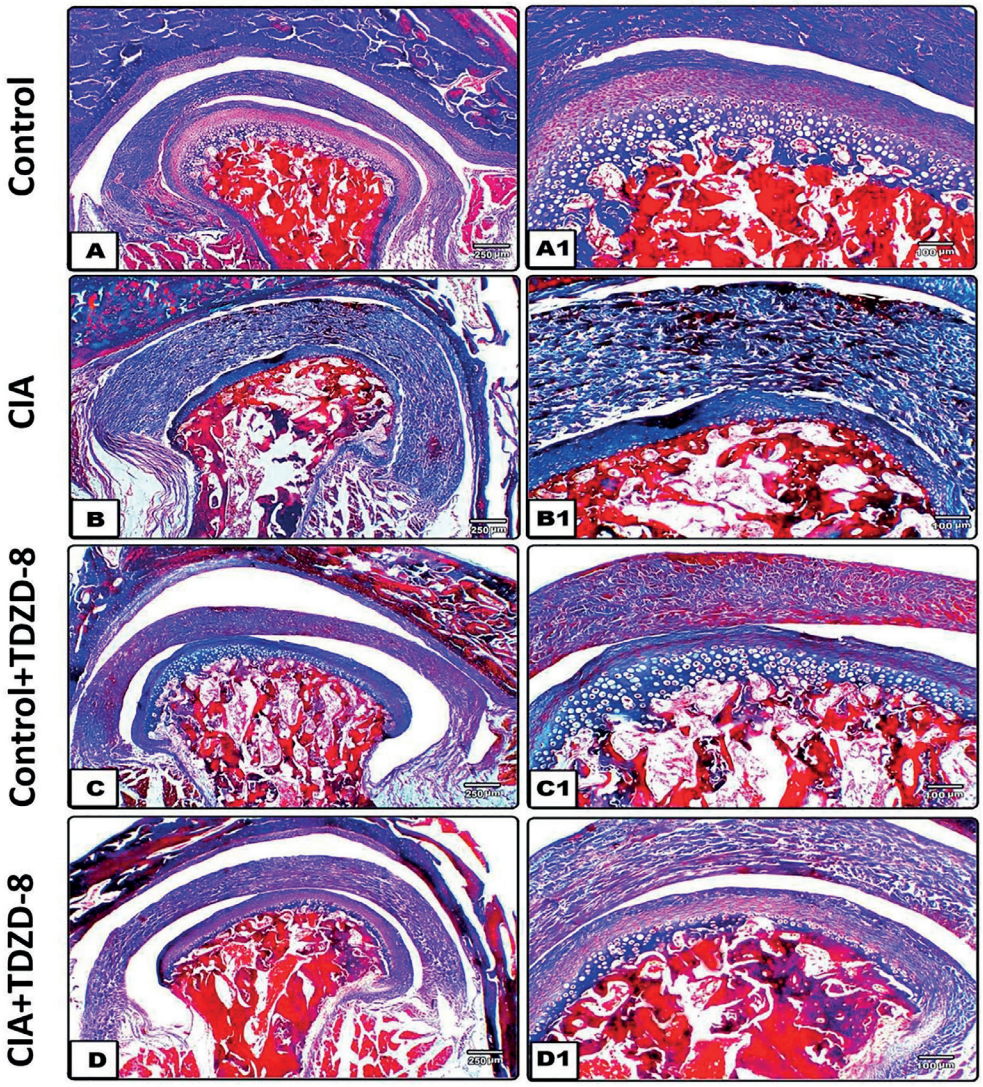

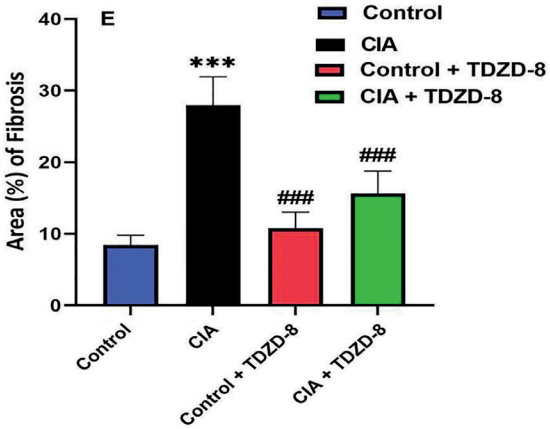

Figure 3. Temporomandibular joint micro-section, Masson's trichrome (MTC) staining. **A-A1**, showing the control group with normal collagen fibers of condylar cartilage arranged in a normal mode. Normal subchondral bone with mineralized regular trabecular bone structures. **B-B1**, In the CIA group, showing a higher intensity of blue-stained disorganized collagen fibers in the articular disc, alterations were more aggravated in the subchondral bone, revealing irregular and disordered trabecular bone structures (stained blue) with large marrow cavities. **C-C1**, shows Control+TDZD-8 treated group, revealed similar collagen distribution of the untreated group. **D-D1**, shows the CIA+TDZD-8 treated group, regenerated collagen fibers in some areas of regenerated cartilage, near a normal arrangement of collagen fibers, was observed around cell lacunae. The images (**A**), (**B**), (**C**), and (**D**) 100 X magnification, while (**A1**), (**B1**), (**C1**), and (**D1**) were 400 X magnification. **E**, a graph showing the collagen fibers (%) area in all groups. Data are shown as the mean (±SD). ***$p < 0.001$ *vs.* control, and $^{###}p < 0.001$ *vs.* CIA.

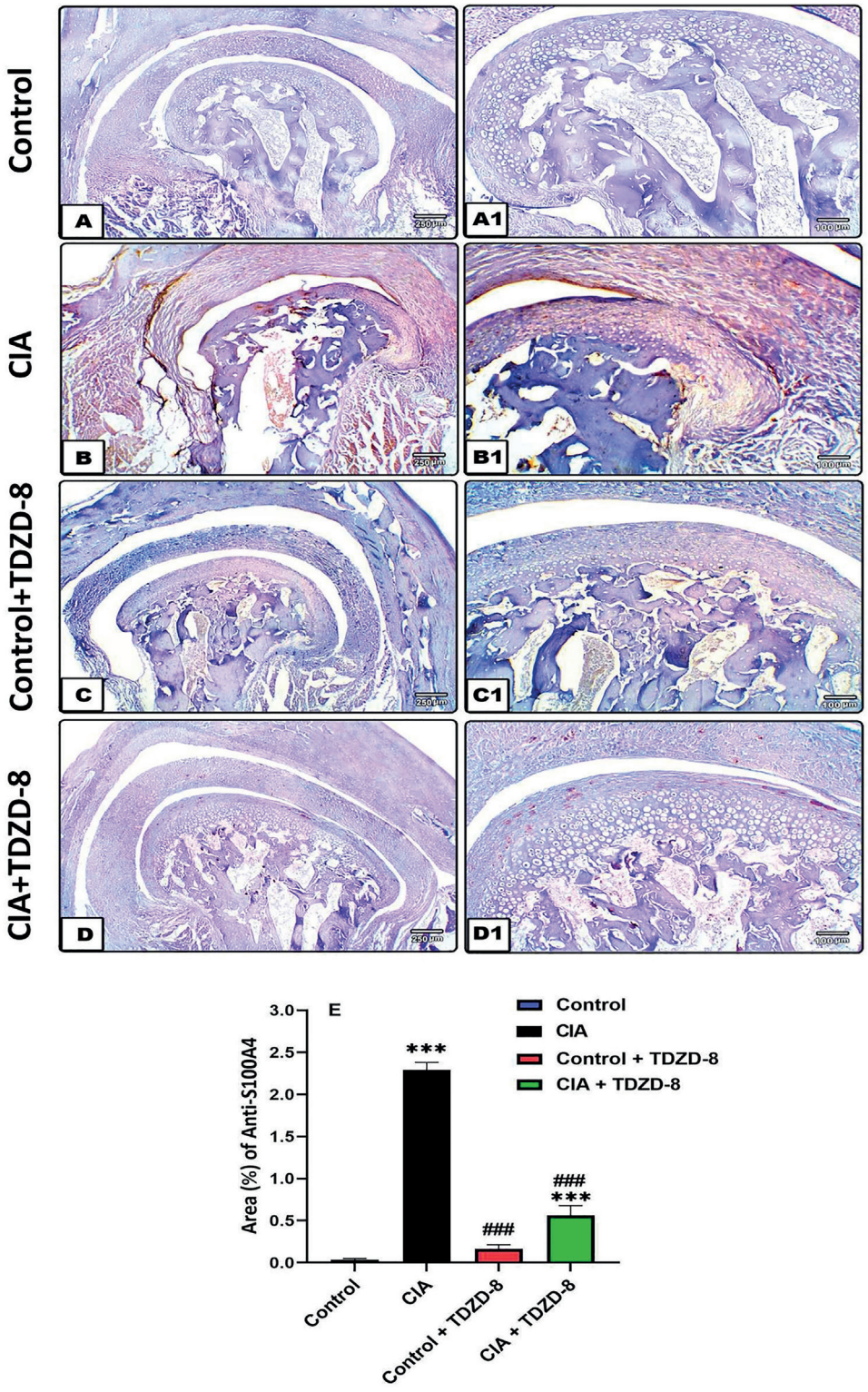

Figure 4. Temporomandibular joint micro-section, anti-S100A4 immunohistochemistry (IHC). **A-A1**, The control group shows a negative immune reaction. **B-B1**, CIA group: shows a moderate immune reaction. **C-C1**, Control+TDZD-8 treated group shows no immune staining. **D-D1**, CIA + TDZD-8 treated group shows a mild immune reaction. The photomicrographs (**A**), (**B**), (**C**), and (**D**) were captured at 100 X magnification, while (**A1**), (**B1**), (**C1**), and (**D1**) were captured at 400 X magnification. **E**, a graph showing the area (%) of anti-S100A4 immunohistochemistry. Data are shown as the mean (±SD). ***$p <$ 0.001 *vs.* control group, and $^{###}p < 0.001$ *vs.* CIA group.

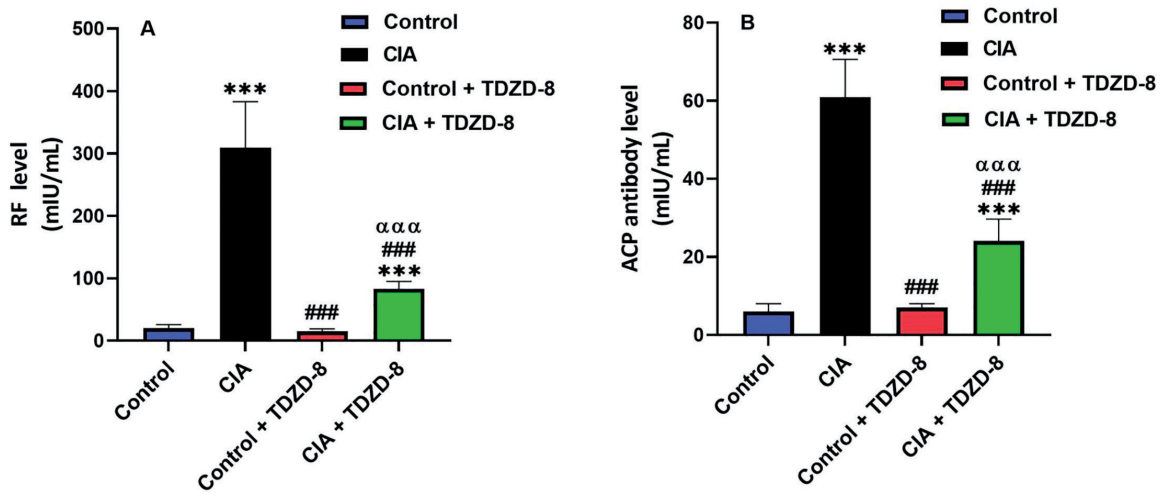

Figure 5. Levels of biochemical markers in serum of rats. **A**, Level of rheumatoid factor (RF, mIU/mL) and **(B)** level of anti-citrullinated protein antibody (ACP-antibody, mIU/mL). Data are displayed as the mean (±SD). ***$p < 0.001$ *vs.* control group, and $^{###}p < 0.001$ *vs.* CIA group, and $^{αααα}p < 0.001$ *vs.* control+TDZD-8 treated group.

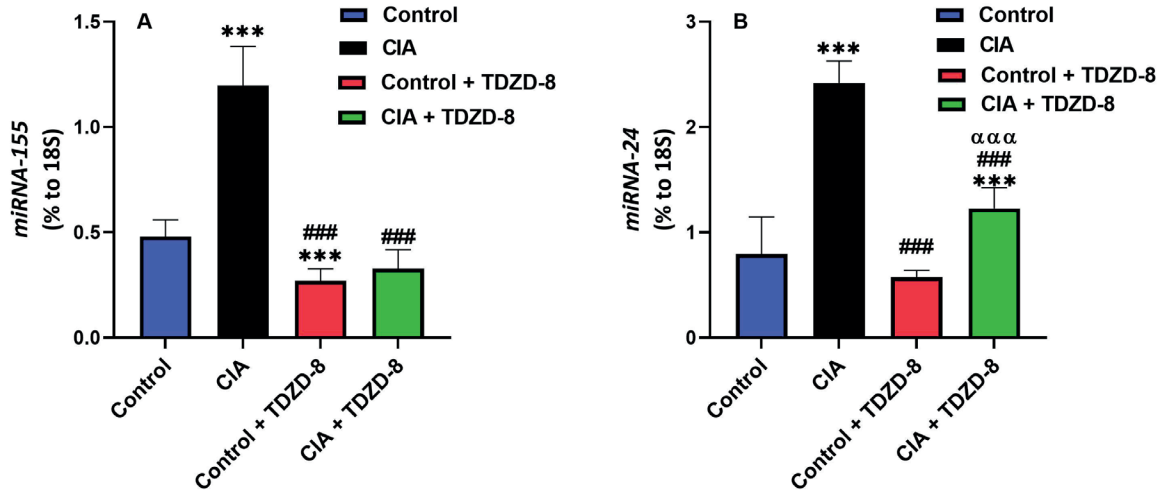

Figure 6. Fold changes of *miRNA-155* **(A)** and *miRNA-24* **(B)** gene expression in all animal groups using RT-PCR analysis. $p < 0.05$ *vs.* CIA. Data are displayed as the mean (±SD). ***$p < 0.001$ *vs.* control group, and $^{###}p < 0.001$ *vs.* CIA group, and $^{αααα}p < 0.001$ *vs.* control+TDZD-8 treated group.

There was a statistically significant difference between mean miRNA-24 levels in the four groups (p-value < 0.001, Effect size $\eta^2 = 0.919$). Pair-wise comparisons using Bonferroni's post-hoc test revealed that the CIA group showed the statistically significantly highest mean miRNA-24 level. CIA+TDZD-8 group showed a statistically significantly decreased mean value. There was no statistically significant difference between the control and control+TDZD-8 groups; both showed the statistically significantly lowest mean miRNA-24 level (Figure 6B).

Discussion

The current work examined the temporomandibular joint in a rat model of collagen-induced rheumatoid arthritis (CIA). Given the similarities in pathology and arthritic manifestations between CIA model animals and individuals with rheumatoid arthritis (RA), the CIA model is the most frequently applied animal model for RA research[35]. We applied this model to investigate the role of S100A4, *miRNA-155*, and *miRNA-24* in the pathophysiology of RA with or without the application of the GSK-3β inhibitor, TDZD-8.

On day 21, the rats in the CIA model group began to exhibit joint abnormalities, swelling, and erythema in their paws. In our study, histochemical analysis by Masson trichrome revealed an increased amount of blue-stained collagen fibers in the articular disc of the CIA group. de Sousa et al[8] found an upsurge in type III collagen in the rats' TMJ RA, indicating an attempt to regenerate the damage to the articular cartilage. We analyzed the blood and temporomandibular joint using ELISA, PCR, and immunohistochemistry. We believe our work is the first to demonstrate the role of S100A4 protein *miRNA-155*, and *miRNA-24* in TMJ RA.

Glycogen synthase kinase 3β (GSK-3β) was primarily recognized as a fundamental regulator of insulin-dependent glycogen synthesis[36]. GSK-3β is also implicated in the regulation of fibrotic and inflammatory processes[37]. Wadhwa et al[38] demonstrated that GSK3-β activity is essential for the full enhancement of proinflammatory mediators' elaboration, such as IL-6, IL-1β, and TNF-α. Additionally, GSK-3β specific inhibitors such as thiadiazolidinone-8 (TDZD-8) significantly attenuate proinflammatory cytokine elaboration and promote the production of anti-inflammatory cytokine[39,40]. It was observed that TDZD-8 in this experimental model attenuates the clinical and morphological manifestations of the disease[23].

RA is a long-lasting inflammatory autoimmune disorder that causes synovial membrane degeneration, cartilage destruction, and bone loss. It is marked by the release of many inflammatory mediators that trigger significant swelling, discomfort, and stiffness in the joints[41,42]. In addition, RF and ACPA are frequent blood indicators linked to RA, and the levels of these markers are correlated with the degree of severity of the condition[43,44]. Our findings ascertained these reports, and the apparent improvement in the arthritis score and mitigation of joint damage brought on by CIA may be explained by a considerable decrease in the levels of these biomarkers after treatment with TDZD-8[23,45]. In the current study, the CIA+TDZD-8 group showed a marked decrease in the mean area of fibrosis. Guo et al[46] reported that TDZD-8 suppressed Aldosterone-induced perivascular cardiac fibrosis. They attributed that to the role of TDZD-8 in the activation of autophagy. The proposed mechanisms by which TDZD-8 stimulates autophagy need further study.

S100 calcium-binding A4 (S100A4), also known as fibroblast-specific protein 1 (Fspl), is one member of the S100 protein family that controls proliferative and inflammatory activities in RA[47]. Patients with RA showed high levels of S100 protein. Additionally, some S100 proteins can be used as biomarkers for RA activity monitoring[48,49]. RA patients had considerably greater levels of the S100A4 protein expression in the knee's synovial membrane[50,51], signifying that S100A4 overexpression positively correlates with RA development[52]. It considerably increases the expression of inflammatory cytokines[50]. S100A4 can also activate synovial fibroblasts and regulate apoptosis[53]. Decreased S100A4 protein might have a role in reducing fibrosis in RA. S100A4 is dysregulated in fibrotic diseases of lung[54], liver[55], kidney[56], and heart[47]. Therefore, our findings that emphasize the induction of S100A4 agree with the above reports.

The substantial role of miR-155 in the pathophysiology of RA has been well recognized over the past few decades[19,57]. *miRNA-155* is a substantial inflammatory molecule identified in peripheral blood mononuclear cells, circulatory macrophages, Fibroblast-like synovial cells, and the joints of RA patients[58]. Additionally, mice lacking *miRNA-155* did not establish CIA, displayed no apparent inflammatory cells in their synovial membranes, and exhibited normal synovial cell proliferation[59]. Therefore, our findings that highlight the induction of *miRNA-155* by CIA are in accordance with the above reports.

However, the crosstalk between GSK-3β, S100 proteins, and miRNAs expression is underestimated. GSK-3β was proven to regulate miRNAs expression in diverse healthy and cancerous cells. This relation has been documented with multiple miRNAs in different cancers, including (*miR-1229*) in breast cancer, (*miR-96*, *miR-182*, and *miR-183*) in gastric cancer, (*miR-26a*) in lung cancer, (*miR-224*) in colorectal cancer, (*miR-940*) in pancreatic cancer, (*miR-769*) in melanoma, (*miR-433*) in bladder cancer, (*miR-15a*) in nasopharyngeal carcinoma, and (*miR-129*) in endometrial cancer[60]. Also, prophylactic or therapeutic administration of TDZD-8 protects against ischemia/reperfusion (I/R) injury in the rat hippocampus with a reduction of infarct size and levels of S100B protein, a marker of cerebral injury. This was linked to a considerable decrease in oxidative stress, apoptosis, and the inflammatory reaction brought on by cerebral I/R[61]. Furthermore, microRNA appears to control the expression of some S100 family members. Choe et al[62] showed that S100A4 is regulated by miRNA-124, as ascertained in our study. Moreover, the suppression of S100A4 in-

duces inhibition of proliferation and invasion of hepatocellular carcinoma (HCC) cells. Also, co-culturing with liver cancer-associated mesenchymal stem cells and ectopic overexpression of S100A4 significantly increased oncogenic *miRNA-155* expression in HCC. *miRNA-155* inhibitor significantly mitigated the invasion-promoting effects of S100A4. This previous report[62] proposes that S100A4 influences HCC cells by controlling *miRNA-155* expression[63].

Conclusions

Our data showed that GSK-3β inhibition caused a significant decrease in miRNAs gene expression and S100A4 protein. Our results demonstrate for the first-time correlation of *miRNA-155* and *miRNA-24* that might be implicated in the onset of TMJ RA. Consequently, the treatment of CIA with GSK inhibitor (TDZD-8) yields encouraging results, which warrant additional research in humans. We predicted that the TDZD-8 might protect against CIA by suppressing *miRNA155*, *miRNA-24*, and S100 protein levels.

Authors' Contributions

Conceptualization, methodology, writing-review and editing, supervision, project administration, funding acquisition, R.H. Al-Serwi, G. Othaman, and M. El-Sherbiny. Analysis, investigation, writing-original preparation, A. F. Dawood. Software, Validation, analysis, and Interpretation of Data A.K. Alhumaidan, H. S. Alharbi, M.E. Almadani, and D.M.A. Elsherbini. All authors read and approved the final version of the manuscript.

Conflicts of Interest

The authors declare that they have no conflict of interest to declare.

Informed Consent

Not applicable.

Ethics Approval

The research design applied in our study meets Animal Research: Reporting of In Vivo Experiments (ARRIVE) guidelines. Animal experiments involved in this research were approved by the Ethical Committee of the Faculty of Pharmacy, Ain Shams University, Cairo, Egypt (6-2020) and conducted following the guiding principle of laboratory research animal species and utilize, issued by the US National Institutes of Health (NIH publication No. 85-23, reviewed 1996).

Funding

The research was supported by Princess Nourah bint Abdulrahman University Researchers Supporting Project number (PNURSP2023R199), Princess Nourah bint Abdulrahman University, Riyadh, Saudi Arabia, and AlMaarefa University, Riyadh, Saudi Arabia.

Data Availability

The datasets used and/or analyzed during the current study are available from the corresponding author upon reasonable request.

Acknowledgments

The Authors would like to thank Princess Nourah bint Abdulrahman University Riyadh, Saudi Arabia, for support of the research through Princess Nourah bint Abdulrahman University Researchers Supporting Project number (PNURSP2023R199), and AlMaarefa University, Riyadh, Saudi Arabia.

ORCID ID

R.H. Al-Serwi: 0000-0002-2121-9269
G. Othaman: 0009-0008-2997-6636
M. El-Sherbiny: 0000-0002-0814-1743
A.F. Dawood: 0000-0001-7646-0909
A.K. Alhumaidan: 0000-0002-1051-1790
H.S. Alharbi: 0000-0001-7873-9815
M.E. Almadani: 0009-0000-8582-5455
D.M.A. Elsherbini: 0000-0001-5262-6134

References

1) Tański W, Świątoniowska-Lonc N, Tomasiewicz A, Dudek K, Jankowska-Polańska B. The impact of sleep disorders on the daily activity and quality of life in rheumatoid arthritis patients–a systematic review and meta-analysis. Eur Rev Med Pharmacol Sci 2022; 26: 3212-3229.
2) Xu WD, Zhang M, Zhang YJ, Ye DQ. IL-33 in rheumatoid arthritis: potential role in pathogenesis and therapy. Hum Immunol 2013; 74: 1057-1060.
3) Bedaiwi M, Almaghlouth I, Omair M. Effectiveness and adverse effects of anakinra in treatment of rheumatoid arthritis: A systematic review. Eur Rev Med Pharmacol Sci 2021; 25: 7833-7839.
4) Mohammed M, Hamad S, Al-Daeoody A, Shehab A, Ahmed O. Effect of dextrose prolotherapy on internal derangement of the temporomandibular joint. Eur Rev Med Pharmacol Sci 2023; 27: 4883-4889.
5) Mustafa MA, Al-Attas BA, Badr FF, Jadu FM, Wali SO, Bawazir YM, Alattas BA, Jadu F. Prevalence and severity of temporomandibular disorders in rheumatoid arthritis patients. Cureus 2022; 14: e21276.

6) Covert L, Mater HV, Hechler BL. Comprehensive management of rheumatic diseases affecting the temporomandibular joint. Diagnostics 2021; 11: 409.

7) Sadura-Sieklucka T, Gębicki J, Sokołowska B, Markowski P, Tarnacka B. Temporomandibular joint problems in patients with rheumatoid arthritis. Reumatologia/Rheumatology 2021; 59: 161-168.

8) de Sousa LM, de Figueiredo Costa AC, Pereira AF, da Silva Martins C, de Oliveira Filho OV, Goes P, Vale ML, Gondim DV. Temporomandibular joint arthritis increases canonical Wnt pathway expression in the articular cartilage and trigeminal ganglion in rats. Bone Rep 2023; 18: 101649.

9) Liu WW, Xu ZM, Li ZQ, Zhang Y, Han B. RANKL, OPG and CTR mRNA expression in the temporomandibular joint in rheumatoid arthritis. Exp Ther Med 2015; 10: 895-900.

10) Kapila S, Lee C, Tavakkoli Jou M, Miller A, Richards D. Development and histologic characterization of an animal model of antigen-induced arthritis of the juvenile rabbit temporomandibular joint. J Dent Res 1995; 74: 1870-1879.

11) Sodhi A, Naik S, Pai A, Anuradha A. Rheumatoid arthritis affecting temporomandibular joint. Contemp Clin Dent 2015; 6: 124.

12) Martinez-Prat L, Nissen MJ, Lamacchia C, Bentow C, Cesana L, Roux-Lombard P, Gabay C, Mahler M. Comparison of serological biomarkers in rheumatoid arthritis and their combination to improve diagnostic performance. Front Immunol 2018; 9: 1113.

13) Mouterde G, Rincheval N, Lukas C, Daien C, Saraux A, Dieudé P, Morel J, Combe B. Outcome of patients with early arthritis without rheumatoid factor and ACPA and predictors of rheumatoid arthritis in the ESPOIR cohort. Arthrit Res Ther 2019; 21: 1-9.

14) Rantapää-Dahlqvist S. Diagnostic and prognostic significance of autoantibodies in early rheumatoid arthritis. Scand J Rheumatol 2005; 34: 83-96.

15) Mohammed S, Shaker O, Mohammed A, Fouad N, Hussein H, Ahmed N, Ahmed O, Ali D, Mohamed M, Ibrahim A. Impact of miR-155 (rs767649 A> T) and miR-146a (rs57095329 A> G) polymorphisms in System Lupus Erythematosus susceptibility in an Egyptian cohort. Eur Rev Med Pharmacol Sci 2021; 25: 1425-1435.

16) Stanczyk J, Pedrioli DML, Brentano F, Sanchez-Pernaute O, Kolling C, Gay RE, Detmar M, Gay S, Kyburz D. Altered expression of MicroRNA in synovial fibroblasts and synovial tissue in rheumatoid arthritis. Arthritis Rheum 2008; 58: 1001-1009.

17) Dawood AF, Younes S, Alzamil NM, Alradini FA, Saja MF. Inhibition of glycogen synthase kinase-3β protects against collagen type II-induced arthritis associated with the inhibition of miR155/24 and inflammation and upregulation of apoptosis in rats. Arch Physiol Biochem 2022; 128: 679-687.

18) Mookherjee N, El-Gabalawy HS. High degree of correlation between whole blood and PBMC expression levels of miR-155 and miR-146a in healthy controls and rheumatoid arthritis patients. J Immunol Methods 2013; 400: 106-110.

19) Churov AV, Oleinik EK, Knip M. MicroRNAs in rheumatoid arthritis: altered expression and diagnostic potential. Autoimmun Rev 2015; 14: 1029-1037.

20) Aguilar-Morante D, Morales-Garcia JA, Sanz-San-Cristobal M, Garcia-Cabezas MA, Santos A, Perez-Castillo A. Inhibition of glioblastoma growth by the thiadiazolidinone compound TDZD-8. PLoS One 2010; 5: e13879.

21) Wang Y, Tong K. Glycogen synthase kinase-3β inhibitor ameliorates imbalance of connexin 43 in an acute kidney injury model. Toxicol Rep 2015; 2: 1391-1395.

22) Martinez A, Castro A, Dorronsoro I, Alonso M. Glycogen synthase kinase 3 (GSK-3) inhibitors as new promising drugs for diabetes, neurodegeneration, cancer, and inflammation. Med Res Rev 2002; 22: 373-384.

23) Zhou H, Liu J, Zeng J, Hu B, Fang X, Li L. Inhibition of GSK-3β alleviates collagen II-induced rheumatoid arthritis in rats. Med Sci Monit 2016; 22: 1047.

24) Grimes CA, Jope RS. The multifaceted roles of glycogen synthase kinase 3β in cellular signaling. Prog Neurobiol 2001; 65: 391-426.

25) Yadav S, Pandey A, Shukla A, Talwelkar SS, Kumar A, Pant AB, Parmar D. miR-497 and miR-302b regulate ethanol-induced neuronal cell death through BCL2 protein and cyclin D2. J Biol Chem 2011; 286: 37347-37357.

26) Brenner AK, Bruserud Ø. S100 proteins in acute myeloid leukemia. Neoplasia 2018; 20: 1175-1186.

27) Gonzalez LL, Garrie K, Turner MD. Role of S100 proteins in health and disease. Biochimica et Biophysica Acta (BBA)-Molecular Cell Research 2020; 1867: 118677.

28) Croia C, Bursi R, Sutera D, Petrelli F, Alunno A, Puxeddu I. One year in review 2019: pathogenesis of rheumatoid arthritis. Clin Exp Rheumatol 2019; 37: 347-357.

29) Yammani RR. S100 proteins in cartilage: role in arthritis. Biochim Biophys Acta 2012; 1822: 600-606.

30) Erlandsson MC, Forslind K, Andersson SE, Lund A, Bokarewa MI. Metastasin S100A4 is increased in proportion to radiographic damage in patients with RA. Rheumatology 2012; 51: 932-940.

31) Brand DD, Latham KA, Rosloniec EF. Collagen-induced arthritis. Nat Protoc 2007; 2: 1269-1275.

32) Cuzzocrea S, Mazzon E, Di Paola R, Muià C, Crisafulli C, Dugo L, Collin M, Britti D, Capu-

ti AP, Thiemermann C. Glycogen synthase kinase-3β inhibition attenuates the degree of arthritis caused by type II collagen in the mouse. Clin Immunol 2006; 120: 57-67.

33) Bancroft J, Stevens A. The Haematoxylin and Eosin: Theory and Practice of Histological Techniques; ch 6. Churchill Livingstone: London, UK 1996; 99-112.

34) Bancroft J, Stevens A. Theory and practice of histological techniques. 2nd (ed.) churchill living stone, Edinburgh. London; 1982.

35) Bai L, Bai Y, Yang Y, Zhang W, Huang L, Ma R, Wang L, Duan H, Wan Q. Baicalin alleviates collagen-induced arthritis and suppresses TLR2/MYD88/NF-κB p65 signaling in rats and HFLS-RAs. Mol Med Report 2020; 22: 2833-2841.

36) Wei J, Wang J, Zhang J, Yang J, Wang G, Wang Y. Development of inhibitors targeting glycogen synthase kinase-3β for human diseases: Strategies to improve selectivity. Eur J Med Chem 2022; 236: 114301.

37) Mirdad TM, Al-Ani B, Aseeri FF, Kamar SS, Mirdad R, AlGilban HM, Haidara MA, Abbas AM, Dawood AF. Suppression of nitrosative stress and inflammation of the knee joint synovium in collagen type II-induced rheumatoid arthritis by the inhibition of glycogen synthase kinase-3ß. Int J Morphol 2022; 40: 84-90.

38) Wadhwa P, Jain P, Jadhav HR. Glycogen synthase kinase 3 (GSK3): Its role and inhibitors. Curr Top Med Chem 2020; 20: 1522-1534.

39) Zhang YD, Ding XJ, Dai HY, Peng WS, Guo NF, Zhang Y, Zhou QL, Chen XL. SB-216763, a GSK-3β inhibitor, protects against aldosterone-induced cardiac, and renal injury by activating autophagy. J Cell Biochem 2018; 119: 5934-5943.

40) Sun A, Li C, Chen R, Huang Y, Chen Q, Cui X, Liu H, Thrasher JB, Li B. GSK-3β controls autophagy by modulating LKB1-AMPK pathway in prostate cancer cells. Prostate 2016; 76: 172-183.

41) Parolini O, Souza-Moreira L, O'Valle F, Magatti M, Hernandez-Cortes P, Gonzalez-Rey E, Delgado M. Therapeutic effect of human amniotic membrane–derived cells on experimental arthritis and other inflammatory disorders. Arthritis Rheumatol 2014; 66: 327-339.

42) Bombardier C, Barbieri M, Parthan A, Zack DJ, Walker V, Macarios D, Smolen JS. The relationship between joint damage and functional disability in rheumatoid arthritis: a systematic review. Ann Rheum Dis 2012; 71: 836-844.

43) Bizzaro N, Bartoloni E, Morozzi G, Manganelli S, Riccieri V, Sabatini P, Filippini M, Tampoia M, Afeltra A, Sebastiani G. Anti-cyclic citrullinated peptide antibody titer predicts time to rheumatoid arthritis onset in patients with undifferentiated arthritis: results from a 2-year prospective study. Arthrit Res Ther 2013; 15: 1-9.

44) Brenner M, Laragione T, Shah A, Mello A, Remmers EF, Wilder RL, Gulko PS. Identification of two new arthritis severity loci that regulate levels of autoantibodies, interleukin-1β, and joint damage in pristane-and collagen-induced arthritis. Arthritis Rheum 2012; 64: 1369-1378.

45) Arioka M, Takahashi-Yanaga F. Glycogen synthase kinase-3 inhibitor as a multi-targeting anti-rheumatoid drug. Biochem Pharmacol 2019; 165: 207-213.

46) Guo F, Xu J, Wu R. Thiadiazolidinone-8, a GSK3 beta inhibitor, ameliorates aldosterone-induced cardiac inflammation and fibrosis by regulating autophagy. Int J Clin Exp Med 2020; 13: 47-55.

47) Qian L, Hong J, Zhang Y, Zhu M, Wang X, Zhang Y, Chu M, Yao J, Xu D. Downregulation of S100A4 alleviates cardiac fibrosis via Wnt/β-catenin pathway in mice. Cell Physiol Biochem 2018; 46: 2551-2560.

48) Wang Q, Chen W, Lin J. The Role of calprotectin in rheumatoid arthritis. J Transl Med 2019; 7: 126-131.

49) Nys G, Cobraiville G, Servais AC, Malaise MG, de Seny D, Fillet M. Targeted proteomics reveals serum amyloid A variants and alarmins S100A8-S100A9 as key plasma biomarkers of rheumatoid arthritis. Talanta 2019; 204: 507-517.

50) Wu YY, Li XF, Wu S, Niu XN, Yin SQ, Huang C, Li J. Role of the S100 protein family in rheumatoid arthritis. Arthrit Res Ther 2022; 24: 1-9.

51) Li Z, Li Y, Liu S, Qin Z. Extracellular S100A4 as a key player in fibrotic diseases. J Cell Mol Med 2020; 24: 5973-5983.

52) Ambartsumian N, Klingelhöfer J, Grigorian M. The multifaceted S100A4 protein in cancer and inflammation. Methods Mol Biol 2019; 1929: 339-365.

53) Uspenskaya YA, Komleva YK, Pozhilenkova EAe, Salmin VVe, Lopatina OgL, Fursov AAe, Lavrent'ev PV, Salmina AB. Ligands of RAGE-proteins: Role in intercellular communication and pathogenesis of inflammation. Vestn Ross Akad Med Nauk 2015; 70: 694-703.

54) Xia H, Gilbertsen A, Herrera J, Racila E, Smith K, Peterson M, Griffin T, Benyumov A, Yang L, Bitterman PB. Calcium-binding protein S100A4 confers mesenchymal progenitor cell fibrogenicity in idiopathic pulmonary fibrosis. J Clin Invest 2017; 127: 2586-2597.

55) Louka ML, Ramzy MM. Involvement of fibroblast-specific protein 1 (S100A4) and matrix metalloproteinase-13 (MMP-13) in CCl4-induced reversible liver fibrosis. Gene 2016; 579: 29-33.

56) Wen J, Jiao B, Tran M, Wang Y. Pharmacological Inhibition of S100A4 Attenuates Fibroblast Activation and Renal Fibrosis. Cells 2022; 11: 2762.

57) Ammari M, Jorgensen C, Apparailly F. Impact of microRNAs on the understanding and treatment of rheumatoid arthritis. Curr Opin Rheumatol 2013; 25: 225-233.

58) Huang RY, Wu JQ, Liu ZH, Sun SL. MicroRNAs in rheumatoid arthritis: what is the latest with regards to diagnostics? Expert Rev Mol Diagn 2019; 19: 363-366.

59) Kurowska-Stolarska M, Alivernini S, Ballantine LE, Asquith DL, Millar NL, Gilchrist DS, Reilly J, Ierna M, Fraser AR, Stolarski B. MicroRNA-155 as a proinflammatory regulator in clinical and experimental arthritis. Proc Natl Acad Sci U S A 2011; 108: 11193-11198.

60) Sahin I, Eturi A, De Souza A, Pamarthy S, Tavora F, Giles FJ, Carneiro BA. Glycogen synthase kinase-3 beta inhibitors as novel cancer treatments and modulators of antitumor immune responses. Cancer Biol Ther 2019; 20: 1047-1056.

61) Rana AK, Singh D. Targeting glycogen synthase kinase-3 for oxidative stress and neuroinflammation: opportunities, challenges and future directions for cerebral stroke management. Neuropharmacology 2018; 139: 124-136.

62) Choe N, Kwon DH, Shin S, Kim YS, Kim YK, Kim J, Ahn Y, Eom GH, Kook H. The micro RNA miR-124 inhibits vascular smooth muscle cell proliferation by targeting S100 calcium-binding protein A4 (S100A4). FEBS Lett 2017; 591: 1041-1052.

63) Yan XL, Jia YL, Chen L, Zeng Q, Zhou JN, Fu CJ, Chen HX, Yuan HF, Li ZW, Shi L. Hepatocellular carcinoma-associated mesenchymal stem cells promote hepatocarcinoma progression: role of the S100A4-miR155-SOCS1-MMP9 axis. Hepatology 2013; 57: 2274-2286.